

Magnetoresistance in paramagnetic heavy fermion metals

D Parihari¹ and N S Vidhyadhiraja²

¹ Department of Physics, Indian Institute of Technology Kharagpur, Kharagpur 721302, India

² Theoretical Sciences Unit, Jawaharlal Nehru Centre for Advanced Scientific Research, Jakkur, Bangalore 560064, India

Received 14 July 2009, in final form 21 August 2009

Published 14 September 2009

Online at stacks.iop.org/JPhysCM/21/405602

Abstract

A theoretical study of magnetic field (h) effects on single-particle spectra and the transport quantities of heavy fermion metals in the paramagnetic phase is carried out. We have employed a non-perturbative local moment approach (LMA) to the asymmetric periodic Anderson model within the dynamical mean field framework. The lattice coherence scale ω_L , which is proportional within the LMA to the spin-flip energy scale, and has been shown in earlier studies to be the energy scale at which crossover to single-impurity physics occurs, increases monotonically with increasing magnetic field. The many body Kondo resonance in the density of states at the Fermi level splits into two, with the splitting being proportional to the field itself. For $h \geq 0$, we demonstrate adiabatic continuity from the strongly interacting case to a corresponding non-interacting limit, thus establishing Fermi liquid behaviour for heavy fermion metals in the presence of a magnetic field. In the Kondo lattice regime, the theoretically computed magnetoresistance is found to be negative in the entire temperature range. We argue that such a result could be understood at $T \gtrsim \omega_L$ by field-induced suppression of spin-flip scattering and at $T \lesssim \omega_L$ through lattice coherence. The coherence peak in the heavy fermion resistivity diminishes and moves to higher temperatures with increasing field. Direct comparison of the theoretical results to the field dependent resistivity measurements in CeB₆ yields good agreement.

1. Introduction

The investigation of lanthanide/actinide based heavy fermion (HF) systems has been a central theme in condensed matter physics both theoretically and experimentally [1]. Their behaviour is quite distinct from conventional clean metals, the basic physics being driven by strong spin-flip scattering from essentially localized f-levels, generating the large effective mass. The periodic Anderson model (PAM) forms the general paradigm within which these materials are studied. The minimal model consists of a regular array of sites, each associated with a localized, non-degenerate f-electron core orbital, coupled to a delocalized conduction electron orbital via a local hybridization. Neighbouring conduction electron orbitals are connected via a hopping matrix element and electron interactions enter the model via an on-site Coulomb repulsion.

The dynamical mean field theory (DMFT) [2] has proved to be a very powerful framework for studies of various lattice models such as the Hubbard model or the PAM. Within DMFT,

which is exact in the limit of infinite dimensions, the self-energy becomes spatially local or momentum independent. As a consequence, lattice models map onto an effective single-impurity Anderson model (SIAM) with a self-consistently determined host [2].

The PAM in the absence of a magnetic field has been studied extensively within the framework of DMFT. Some of the numerical or semi-analytical methods (impurity solvers) that exist for solving the effective SIAM that arises within DMFT are quantum Monte Carlo [3], numerical renormalization group [4], iterated perturbation theory [5], noncrossing approximation [6], the local moment approach [7, 8], the large- N /slave-boson [9], exact diagonalization [10], self-consistent perturbation theory [11], the Gutzwiller variational method [12] and the average T -matrix approximation [13]. Every method has its own advantage, however most of them suffer from one or the other limitations. For example, the QMC suffers from a minus sign problem at low temperature or large interactions, while IPT is able to capture only an algebraic decay of the Kondo scale with increasing interactions. ED and

NRG are in principle exact, as is QMC, but since the spectral functions are obtained as a set of discrete poles, a broadening is required, which is non-uniquely specified.

In this context, the local moment approach (LMA) [8, 14–18], a diagrammatic theory based non-perturbative many body method, has emerged as an approach for the single-impurity model and even for the lattice models within DMFT, that overcomes some of the limitations mentioned above. In particular, one obtains the exact dependence on interactions and hybridization of the Kondo scale of the SIAM in strong coupling as the Bethe ansatz solution for the Kondo model [14]. Very good agreement has been seen between LMA and NRG results for the spectral functions of the SIAM [17, 18]. Within DMFT, the LMA has proved quite successful in describing the spectral and transport properties of several metallic and insulating heavy fermion systems such as CeB₆, SmB₆, YbAl₃, CeAl₃, YbB₁₂, CeOs₄Sb₁₂ in the paramagnetic phase [19–21]. The LMA is computationally inexpensive, yields quantities in real frequency directly, and is semi-analytical. One limitation of LMA is that it is based on a symmetry restoration ansatz, that is not easily generalizable to other problems, such as the multi-orbital or multi-channel cases. Recently, a generalization of LMA has been reported for the multi-orbital Anderson and Hubbard model [22]. Further, it was shown that the LMA is a conserving approximation. The other limitation is that since LMA is an approximate theory, one has to benchmark its results against more exact theories such as NRG and QMC to ascertain its reliability. Nevertheless, given the several advantages above, and benchmarks, the LMA within DMFT is an appropriate choice to study the effects of magnetic fields in heavy fermions.

Several theoretical studies of the effects of magnetic field on heavy fermion systems using either the Kondo lattice model (KLM) or the PAM have been reported. The magnetic field-induced insulator–metal transition in Kondo insulators has been studied by various groups [23–25]. As relevant to heavy fermion metals, the metamagnetic transition has been studied using large- N mean field [26] and subsequently using DMFT + QMC [27]. In this work, our objective is to understand magnetotransport in heavy fermion metals. Previous work in this direction has been carried out mainly either using the single-site Anderson models [28], thus missing out the lattice coherence effects completely, or using the large- N mean field treatment of the Anderson lattice Hamiltonian [29]. In order to capture the lattice coherence effects along with the single-impurity incoherent regime, quantitatively within a single framework, we employ the finite field LMA [17, 18, 25] within DMFT for the periodic Anderson model away from half-filling and determine the effect of a magnetic field on the spectra and the transport of heavy fermion metals. Our focus has been on the strong coupling regime, and the quantities that we have studied are spectral functions and magnetoresistance. The paper is organized as follows; the model and formalism are presented in section 2, followed, in section 3 by results for the field evolution of single-particle dynamics and dc transport. In section 4, the experimental magnetoresistance of CeB₆ is compared with theory; and finally we conclude with a brief summary.

2. Model and formalism

The Hamiltonian for the PAM in standard notation is given by:

$$\hat{H} = -t \sum_{(i,j),\sigma} c_{i\sigma}^\dagger c_{j\sigma} + \sum_{i\sigma} \left(\epsilon_f + \frac{U}{2} f_{i-\sigma}^\dagger f_{i-\sigma} \right) f_{i\sigma}^\dagger f_{i\sigma} + V \sum_{i\sigma} (f_{i\sigma}^\dagger c_{i\sigma} + \text{h.c.}) + \sum_{i\sigma} \epsilon_c c_{i\sigma}^\dagger c_{i\sigma}. \quad (2.1)$$

The first term describes the kinetic energy of the non-interacting conduction (c) band due to nearest neighbour hopping t . The second term refers to the f-levels with site energies ϵ_f and on-site repulsion U , while the third term describes the c/f hybridization via the local matrix element V . The final term represents the c-electron orbital energy. In the limit of large dimensions, the hopping needs to be scaled as $t \propto t_*/\sqrt{Z}$, where Z is the lattice coordination number. We consider the hypercubic lattice, for which the non-interacting density of states is an unbounded Gaussian ($\rho_0(\epsilon) = \exp(-\epsilon^2/t_*^2)/(\sqrt{\pi}t_*)$). Particle–hole asymmetry in the PAM could be introduced in two ways [8]: (i) through an asymmetric conduction band, i.e. $\epsilon_c \neq 0$, or (ii) through an asymmetric f-level, $\epsilon_f \neq -\frac{U}{2}$. In general, we may quantify the f-level asymmetry by defining $\eta = 1 + \frac{2\epsilon_f}{U}$, such that $\eta = 0$ is equivalent to particle–hole symmetric f-levels. Our primary interest is in the strong coupling Kondo lattice regime ($n_f \rightarrow 1$) but with arbitrary conduction band filling (n_c).

Within DMFT, the PAM may be mapped onto an effective self-consistent impurity problem within DMFT. We choose the local moment approach to solve the effective impurity problem arising within DMFT. For details of the LMA developed for use within DMFT in the absence of a field, the reader is referred to some of our previous work [8, 19–21]. Magnetic field effects in the symmetric PAM as appropriate to Kondo insulators was recently studied by us [25]. As discussed in that work, the presence of a global magnetic field results in the Zeeman splitting of the bare electronic energy levels as $\epsilon_{\gamma\sigma} = \epsilon_\gamma - \sigma h_\gamma$, for $\gamma = c$ and f-electrons. Here $h_\gamma = \frac{1}{2} g_\gamma \mu_B H$ and μ_B is the Bohr magneton; the constants g_f and g_c are the electronic g-factors for the f- and c-electrons respectively. Although $g_f \neq g_c$ in general, for simplicity we set $g_f = g_c$. The degeneracy of the symmetry broken solutions at the mean field level (denoted by A and B) is lifted by a magnetic field. We consider here $h > 0$ for which $+|\mu(h)|$ (A-type) is the sole solution. The Feenberg self-energy [8, 19, 25] becomes a functional solely of the A-type Green’s function, i.e. $S_\sigma(\omega) \equiv S_\sigma[G_{A\sigma}^c]$. Since the B-type solution does not exist, the label ‘A’ will be implicit in the following.

In presence of a uniform magnetic field, the LMA Green functions are given by

$$G_\sigma^c(\omega, T, h) = \left[\omega^+ + \sigma h - \epsilon_c - S_\sigma^c[G_\sigma^c] - \frac{V^2}{\omega^+ + \sigma h - \epsilon_f - \tilde{\Sigma}_\sigma(\omega, T, h)} \right]^{-1} \quad (2.2)$$

$$G_\sigma^f(\omega, T, h) = \left[\omega^+ + \sigma h - \epsilon_f - \tilde{\Sigma}_\sigma(\omega, T, h) - \frac{V^2}{\omega^+ + \sigma h - \epsilon_c - S_\sigma^c[G_\sigma^c]} \right]^{-1} \quad (2.3)$$

with $G^\gamma(\omega) = \frac{1}{2} \sum_\sigma G_\sigma^\gamma(\omega)$. The self-energy can be written as a sum of the static and dynamic parts as,

$$\tilde{\Sigma}_\sigma(\omega, T, h) = \frac{U}{2} (\bar{n} - \sigma |\bar{\mu}|(T, h)) + \Sigma_\sigma(\omega, T, h) \quad (2.4)$$

where $|\bar{\mu}|(T, h)$ is the UHF local moment in presence of a magnetic field and temperature. The dynamical self-energy within the LMA is given by [16, 25]

$$\begin{aligned} \Sigma_{-\sigma}(\omega, T, h) &= U^2 \int_{-\infty}^{\infty} \int_{-\infty}^{\infty} d\omega_1 d\omega_2 \chi^{-\sigma\sigma}(\omega_1, T, h) \\ &\times \frac{\mathcal{D}_\sigma(\omega_2, h)}{\omega^+ + \omega_1 - \omega_2} h(\omega_1; \omega_2) \end{aligned} \quad (2.5)$$

$$h(\omega_1; \omega_2) = \theta(-\omega_1)[1 - f(\omega_2, T)] + \theta(\omega_1)f(\omega_2, T)$$

where $\chi^{-\sigma\sigma}(\omega, T, h) = \pi^{-1} \text{Im} \Pi^{-\sigma\sigma}(\omega, h)$, $f(\omega) = [\exp^{\beta\omega} + 1]^{-1}$ is the Fermi function and $\theta(\omega)$ is the Heaviside step function. Here, $\Pi^{-\sigma\sigma}(\omega, T, h)$ denotes the transverse spin polarization propagator which can be expressed as $\Pi^{+-} = {}^0\Pi^{+-}/(1 - U {}^0\Pi^{+-})$, where ${}^0\Pi^{+-}$, the bare p-h bubble, is constructed using the field dependent mean field spectral densities [14, 20]. The host spectral function is given by $\mathcal{D}_\sigma(\omega, h) = -\frac{1}{\pi} \text{Im} \mathcal{G}_\sigma(\omega, h)$; where the host/medium Green's function \mathcal{G}_σ is given by

$$\mathcal{G}_\sigma(\omega, T, h) = \left[\omega^+ - e_f + \sigma x + \sigma h - \frac{V^2}{\omega^+ - \epsilon_c + \sigma h - \mathcal{S}^c(\omega, T, h)} \right]^{-1} \quad (2.6)$$

where the parameters $x = U|\mu|/2$ and e_f are determined at $h, T = 0$ by satisfying the symmetry restoration condition

$$\Sigma_\uparrow^R(\omega = 0; e_f, x) - \Sigma_\downarrow^R(\omega = 0; e_f, x) = U|\bar{\mu}(e_f, x)| \quad (2.7)$$

and Luttinger's integral theorem [8, 30]

$$I_L(e_f, x) = \text{Im} \int_{-\infty}^0 \frac{d\omega}{\pi} \frac{\partial \Sigma(\omega)}{\partial \omega} G^f(\omega) = 0 \quad (2.8)$$

which in turn ensures a Fermi liquid ground state. Note that e_f is distinct from ϵ_f . The latter is a 'bare' model parameter while the former is a derived 'shifted chemical potential', which is determined through the imposition of the Luttinger's integral, or equivalently the Friedel sum rule [8]. In practice however, it is more convenient numerically to fix x and e_f at the outset and treat U and ϵ_f as unknown parameters to be determined by the above two conditions [8]. As input for the calculation at a given field/temperature, we use the self-energies and Green's functions of a lower field/temperature.

In the limit of infinite dimensions, vertex corrections in the skeleton expansion for the current-current correlation function are absent, hence a knowledge of single-particle dynamics is sufficient within DMFT to determine $\mathbf{q} = 0$ transport properties. For $h > 0$, the d -dimensional isotropic conductivity is computed by adding the contributions from each of the spin channels as

$$\begin{aligned} \bar{\sigma}(\omega, T, h) &= \frac{\sigma_0 t_*^2}{d\omega} \sum_\sigma \int_{-\infty}^{\infty} d\omega_1 [f(\omega_1) - f(\omega_1 + \omega)] \\ &\times \langle D_\sigma^c(\epsilon; \omega_1) D_\sigma^c(\epsilon; \omega_1 + \omega) \rangle_\epsilon \end{aligned} \quad (2.9)$$

where $\sigma_0 = \frac{\pi e^2}{\hbar a}$ (a is the lattice parameters) and $D_\sigma^c(\epsilon; \omega) = -\frac{1}{\pi} \text{Im} G_\sigma^c(\epsilon; \omega)$. The lattice c -Green's function is given by $G_\sigma^c(\epsilon; \omega) = [\gamma_\sigma(\omega, T, h) - \epsilon]^{-1}$ where

$$\gamma_\sigma = \omega^+ + \sigma h - \epsilon_c - V^2(\omega^+ + \sigma h - \epsilon_f - \tilde{\Sigma}_\sigma(\omega, T, h))^{-1},$$

and the ϵ -average is defined by

$$\langle A(\epsilon; \omega) \rangle_\epsilon = \int_{-\infty}^{\infty} d\epsilon \rho_0(\epsilon) A(\epsilon; \omega). \quad (2.10)$$

We now proceed to discuss the results obtained by implementing the finite field and finite temperature LMA.

3. Results and discussions

In this section, we will discuss the single-particle dynamics and transport in the presence of a magnetic field using LMA. Our primary focus is on the strong coupling Kondo lattice regime (where $n_f \rightarrow 1$, but n_c is arbitrary). Before discussing the finite field calculations, we will review a few well established concepts. At $T = 0$ and $h = 0$ [8], the strong coupling Kondo lattice regime is characterized by an exponentially small (in strong coupling) low energy scale $\omega_L = ZV^2/t_*$. The single-particle properties of the asymmetric PAM exhibit universal scaling in terms of ω/ω_L and for a fixed ϵ_c/t_* and η . For finite- T and $h = 0$, the spectra $D^c(\omega)$ and $V^2 D^f(\omega)$ exhibit scaling in terms of ω/ω_L and T/T_L ($T_L = \omega_L$). In summary, the spectra and transport properties of the PAM are universal functions of ω/ω_L and T/ω_L , for a given conduction band filling and f-level asymmetry; thus being independent of the bare U/t_* and V/t_* . In this context, it is important to mention that the universal form of the scaling functions does depend, albeit weakly, on the specific lattice, which manifests in the bare conduction band density of states. The application of magnetic field does not destroy this universality as shown in a recent work on the symmetric PAM ($T = 0$) where such scaling in terms of $\tilde{\omega}_h = \omega t_*/(Z(h)V^2)$ for a fixed effective field (detailed description is in [25]) was shown to hold good in the presence of a field as well.

To see if such scaling occurs for the asymmetric case, we carry out a low frequency Fermi liquid analysis of the Green's functions by expanding the self-energy about the Fermi level to first order in ω as

$$\Sigma_\sigma^R(\omega, h) = \Sigma_\sigma^R(0, h) + \left(1 - \frac{1}{Z_\sigma(h)}\right) \omega. \quad (3.1)$$

Substituting equation (3.1) in equations (2.2) and (2.3), we find that the spin dependent spectral functions are just renormalized versions of their non-interacting counterparts and are given by (neglecting the 'bare' terms h and ω in the strong coupling limit)

$$D_\sigma^c(\omega; h) \xrightarrow{\omega \rightarrow 0} \rho_0 \left(-\epsilon_c - \frac{1}{\tilde{\omega}_{h\sigma} - \tilde{\epsilon}_f^* + \sigma h_{\text{eff}}^\sigma} \right) \quad (3.2)$$

$$D_\sigma^f(\omega; h) \xrightarrow{\omega \rightarrow 0} \frac{t_*^2}{V^2(\tilde{\omega}_{h\sigma} - \tilde{\epsilon}_f^* + \sigma h_{\text{eff}}^\sigma)^2} D_\sigma^c(\omega; h) \quad (3.3)$$

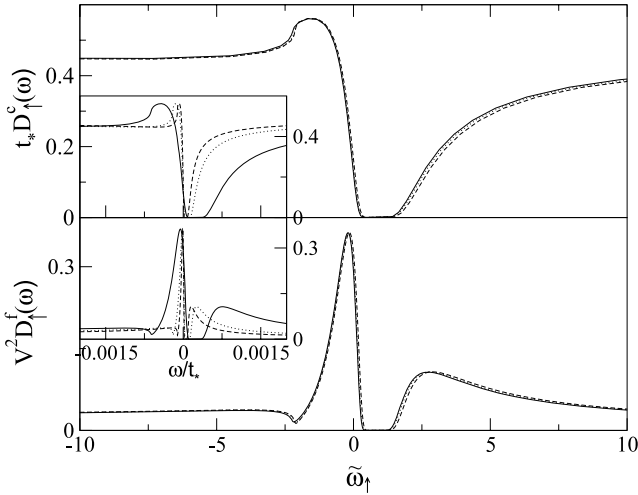


Figure 1. Insets: LMA spin dependent conduction and f-electron spectra versus bare frequency ω/t_* for $\epsilon_c = 0.3t_*$, $\eta \rightarrow 0$, $V^2 = 0.2t_*^2$ and $T = 0$ for three parameter sets: $U \sim 5.1t_*$ and $\tilde{h} = 0.3$ (solid), $U \sim 6.1t_*$ and $\tilde{h} = 0.25$ (dotted), $U \sim 6.6t_*$ and $\tilde{h} = 0.24$ (dashed), for fixed $h_{\uparrow}^{\text{eff}} = 0.39$ (where $\tilde{h} = ht_*/(Z(0)V^2)$). Main: The same spectra when plotted versus $\tilde{\omega}_{h\uparrow} = \omega t_*/(Z_{\uparrow}(h)V^2)$ collapse into one single universal form.

where $\tilde{\omega}_{h\sigma} = \omega t_*/(Z_{\sigma}(h)V^2)$ and the renormalized f-level ($\tilde{\epsilon}_f^*$) and h_{σ}^{eff} can be expressed as,

$$\tilde{\epsilon}_f^* = \frac{t_*}{V^2} \left(\epsilon_f + \frac{U\bar{n}}{2} - \frac{\sigma U \bar{\mu}}{2} + \Sigma_{\sigma}^R(0, 0) \right) \quad (3.4)$$

and

$$h_{\sigma}^{\text{eff}} = \frac{t_*}{V^2} (h - \sigma(\Sigma_{\sigma}^R(0, h) - \Sigma_{\sigma}^R(0, 0))). \quad (3.5)$$

Using the SR condition, equation (2.7), it is easy to see that the effective f-level, $\tilde{\epsilon}_f^*$ is spin independent. Note that the quantities thus defined, namely, $\tilde{\omega}_{h\sigma}$, $\tilde{\epsilon}_f^*$ and h_{σ}^{eff} are dimensionless.

From equations (3.2) and (3.3), we can infer the following: (i) the spin dependent spectra $D_{\sigma}^c(\omega, h)$ and $V^2 D_{\sigma}^f(\omega, h)$ should exhibit scaling in terms of $\tilde{\omega}_{h\sigma}$ for a fixed h_{σ}^{eff} i.e., for a fixed h_{σ}^{eff} , if we plot the spin dependent spectra versus $\tilde{\omega}_{h\sigma}$ for different values of U , they should collapse onto a single curve at the low energy regions for a particular h_{σ}^{eff} . This is shown in figure 1 where in the insets, the conduction electron spectra for up spin (top panel) and the f-electron spectra for up spin (bottom panel) are plotted as a function of the bare frequency ω/t_* with $\epsilon_c = 0.3t_*$, $\eta \rightarrow 0$, $V^2 = 0.2t_*^2$ and $T = 0$ for three parameter sets: $U \sim 5.1t_*$ and $\tilde{h} = 0.3$ (solid), $U \sim 6.1t_*$ and $\tilde{h} = 0.25$ (dotted), $U \sim 6.6t_*$ and $\tilde{h} = 0.24$ (dashed), such that $h_{\uparrow}^{\text{eff}} = 0.39$ is fixed (where $\tilde{h} = ht_*/(Z(0)V^2)$). In the main panel the same spectra are plotted as a function of $\tilde{\omega}_{h\uparrow}$. We see that when we plot the spectra versus bare frequency, they appear very different, but when plotted versus $\tilde{\omega}_{h\uparrow}$ (main panel: top and bottom), they collapse onto a single universal form. We have checked that similar universality also holds for the down spin for a fixed $h_{\downarrow}^{\text{eff}}$.

(ii) The spin dependent conduction and f-electron spectra $D_{\sigma}^c(\omega)$ and $V^2 D_{\sigma}^f(\omega)$ should adiabatically connect to the non-

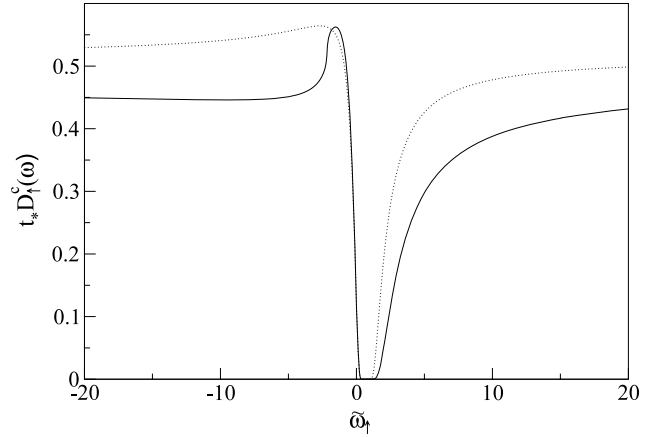


Figure 2. LMA spin dependent scaling spectra (solid lines) are superposed onto the corresponding non-interacting spectra (dotted lines) for a fixed $h_{\uparrow}^{\text{eff}} = 0.45$ and $\tilde{\epsilon}_f^* = 1.09$.

interacting limit at low energy scales i.e., if we take the c-electron and f-electron fields as zero and h_{σ}^{eff} respectively, substitute for ϵ_f the renormalized f-level ($\tilde{\epsilon}_f^*$) and compute the spectra in the non-interacting limit; then the interacting spectra and the non-interacting spectra should be same at low energy scales. This is shown in figure 2, where the spin dependent scaling spectra $D_{\uparrow}^c(\omega)$ for the interacting case ($U = 6.6t_*$) is superposed onto the non-interacting spectra. We see from figure 2 that both the curves are almost identical near the Fermi level. This demonstrates adiabatic continuity of the strong coupling regime to the non-interacting limit which represents Fermi liquid behaviour in the presence of a magnetic field for the asymmetric case (in parallel to the symmetric PAM [25]).

To see the effect of magnetic field on the spin dependent effective fields h_{σ}^{eff} and the spin dependent quasiparticle weights Z_{σ} , we have plotted in figure 3, the spin dependent effective fields ($h_{\uparrow}^{\text{eff}}$ and $h_{\downarrow}^{\text{eff}}$) versus \tilde{h} (left panel) and the spin dependent quasiparticle weights ($Z_{\uparrow}(h)$ and $Z_{\downarrow}(h)$) versus \tilde{h} (right panel). We see that $Z_{\uparrow}(h) \cong Z_{\uparrow}(h)$ and $h_{\uparrow}^{\text{eff}} \cong h_{\downarrow}^{\text{eff}}$ up to about $\tilde{h} \sim 10.0$. So, we can assume the spin summed spectra $D^c(\omega)$ and $V^2 D^f(\omega)$ also should exhibit scaling in terms of $\tilde{\omega}_{h\sigma}$ for low fields (up to $\tilde{h} \sim 10$) for a fixed h_{σ}^{eff} . To see this, we plot spin scaling spectra (main panel) as well as the corresponding spin summed spectra in figure 4 (insets) for $U = 5.1t_*$ (solid line) and $U = 6.6t_*$ (dotted line) for a fixed $h_{\uparrow}^{\text{eff}} = 4.2$ ($\tilde{h} \sim 10.0$) and $T = 0$. Indeed, we see that the spin summed spectra also exhibit universal scaling and adiabatic continuity at low energy scales. We wish to reiterate the discussion in the beginning of this section that the universality and scaling demonstrated above holds for a fixed conduction band filling n_c , a fixed f-level asymmetry and for a specific bare conduction band density of states. In other words, the functional forms of the spectra shown above would change for a different choice for n_c or η or $\rho_0(\epsilon)$.

Now we turn to the LMA results for the field evolution of the asymmetric PAM for a fixed temperature. In figure 5, we show $T = 0$ spin summed conduction and f-electron scaling spectra for various fields: $\tilde{h} = 0$ (solid), 0.5 (dotted), 1.0 (dashed), 1.5 (dot-dashed), 2.0 (bold solid), 3.0 (bold

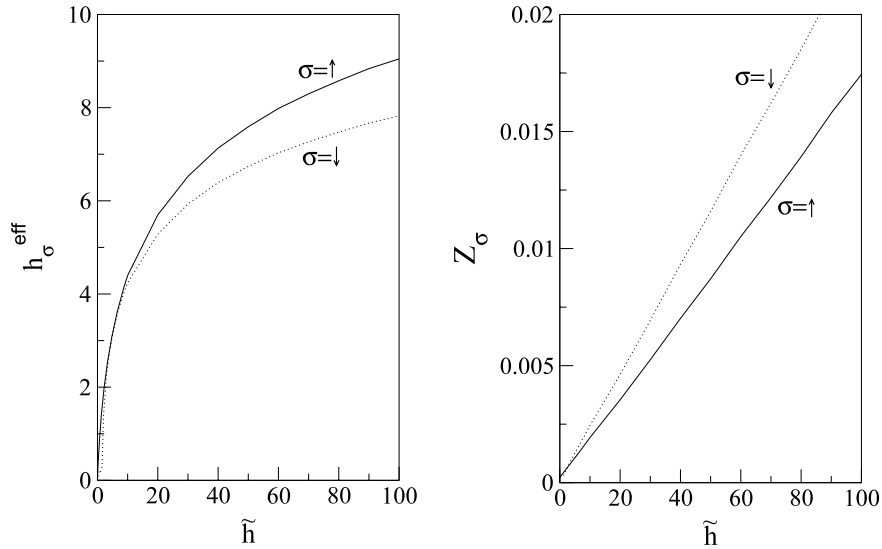


Figure 3. Left panel: h_σ^{eff} versus $\tilde{h} = ht_*/(ZV^2)$ (Z is the quasiparticle weight for $h = 0$) for $\epsilon_c = 0.3t_*$, $\eta \rightarrow 0$, $T = 0$ and $U = 6.6t_*$. Right panel: spin dependent quasiparticle weight $Z_\sigma(h)$ versus \tilde{h} for the same parameters.

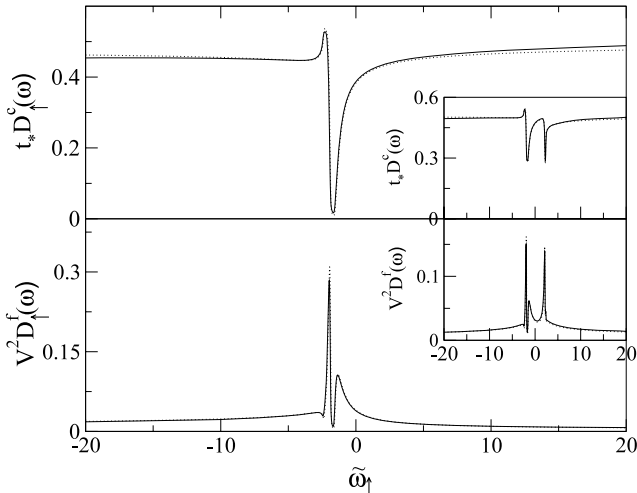


Figure 4. Main panel: LMA up spin conduction electron scaling spectra (top) and up spin f-electron scaling spectra (bottom) versus $\tilde{\omega}_{h\uparrow}$ for $\epsilon_c = 0.3t_*$, $\eta \rightarrow 0$ and $V^2 = 0.2t_*^2$ for two parameter sets: $U \sim 5.1t_*$ and $\tilde{h} = 10.0$ (solid), $U \sim 6.6t_*$ and $\tilde{h} = 9.0$ (dotted) for fixed $h_\uparrow^{\text{eff}} = 4.2$. Insets: the corresponding spin summed conduction and (top) f-electron (bottom) scaling spectra versus $\tilde{\omega}_{h\uparrow}$ for the same parameter sets. Spin summed as well as the spin dependent spectra exhibit universality/scaling in the strong coupling regime.

dotted), 5.0 (bold dashed) and 10.0 (bold dot-dashed) and fixed interaction strength $U = 6.6t_*$. In our earlier work on the symmetric PAM [25], we have shown that there is a gap at the Fermi level, as there must be for a Kondo insulator. But in the asymmetric limit $\epsilon_c = 0.3t_*$, $h = 0$ (see figure 5), the gap moves away from the Fermi level and becomes a pseudogap. The width of the Kondo resonance at the Fermi level is proportional to the low energy scale $\omega_{L\sigma} = Z_\sigma(0)V^2$. The insets of figure 5 show the spectra on a large frequency scale. It is seen that for very large frequencies the tails of the spectra for all fields are identical, which is physically natural since one

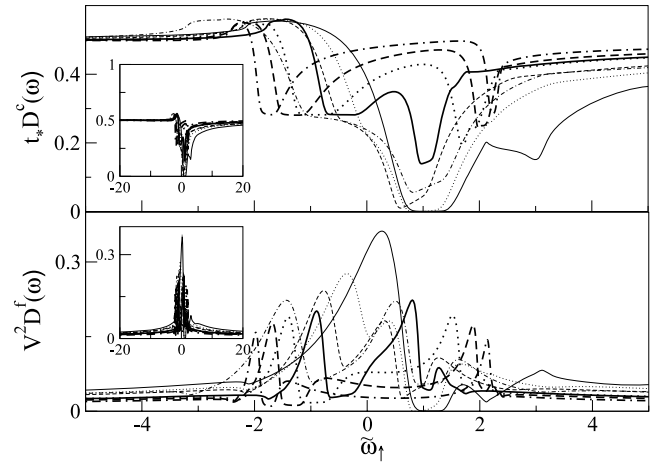


Figure 5. LMA conduction and f-electron spectra versus $\tilde{\omega}_{h\uparrow} = \omega t_*/(Z_\uparrow(h)V^2)$ for $U = 6.6t_*$, $\epsilon_c = 0.3t_*$ and $\eta \rightarrow 0.0$ for $\tilde{h} = 0$ (solid), $\tilde{h} = 0.5$ (dotted), 1.0 (dashed), 1.5 (dot-dashed), 2.0 (bold solid), 3.0 (bold dotted), 5.0 (bold dashed) and 10.0 (bold dot-dashed) for $T = 0$.

can expect that the effect of the field should dominate only for $|\tilde{\omega}_\sigma| \lesssim ht_*/(Z_\sigma(h)V^2)$. Now with increasing magnetic field, the lattice Kondo resonance splits into two peaks, with the distance between the peaks also increasing. Qualitatively we can understand the results as follows: in the non-interacting limit for the symmetric case, we have shown that the c and f-levels shift rigidly due to the Zeeman effect. The same concept is valid for the asymmetric case also for the non-interacting limit i.e. the spectral function for the up and down spin bands shift rigidly away from the Fermi level. In the presence of interactions, in parallel to the symmetric case, the shift of the spin bands should not be rigid due to the competition between Zeeman splitting and Kondo screening. And indeed, we find that although the distance between the two peaks varies linearly with field in strong coupling (see figure 6), the

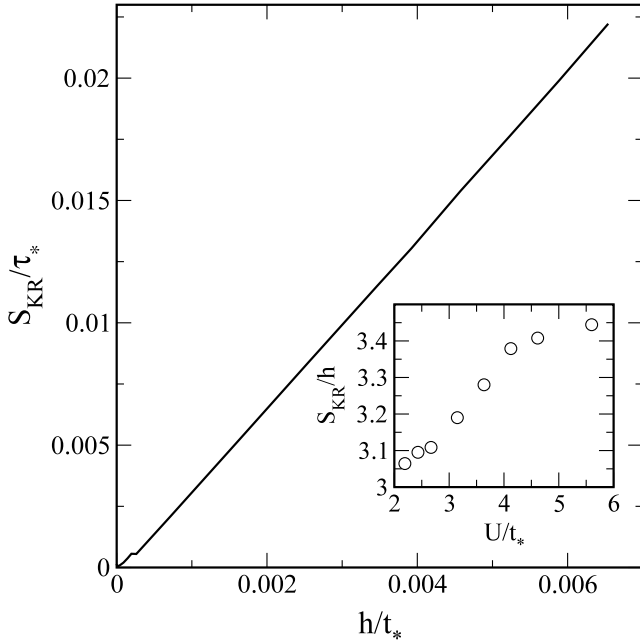


Figure 6. Splitting of the Kondo resonance versus field for $U = 5.5t_*$ and $\epsilon_c = 0.5$, $V^2 = 0.2t_*^2$. The slope of the line in the main panel, i.e. S_{KR}/h as a function of interaction strength U is shown in the inset.

slope is not equal to 2 as it would have been if the shift had been rigid (or purely due to the Zeeman effect). In fact, the slope should be equal to 4 as the following argument shows. From equations (3.2)–(3.5), it is straightforward to see that the splitting of the Kondo resonance, S_{KR} , is given by

$$S_{KR} = \sum_{\sigma} Z_{\sigma}(h)[h - \sigma(\Sigma_{\sigma}^R(0, h) - \Sigma_{\sigma}^R(0, 0))]. \quad (3.6)$$

The strong coupling asymptotic behaviour of the above quantity may be inferred using the expressions derived in [17] for the flat-band SIAM.

$$\Sigma_{\sigma}^R(0, h) - \Sigma_{\sigma}^R(0, 0) = -\frac{4\Delta_0\sigma}{\pi} \ln \left[\frac{Z_{\sigma}(h)}{Z_{\sigma}(0)} \right] \quad (3.7)$$

$$\frac{Z_{\sigma}(h)}{Z_{\sigma}(0)} = 1 + \frac{\pi}{2} \frac{h}{\Delta_0 Z_{\sigma}(0)} \quad (3.8)$$

where $\Delta_0 = \pi V^2 \rho_0(0)$ is the flat-band hybridization. Although these were derived for the SIAM, we are justified in using the same expressions for the PAM for the following reason: since the transverse spin polarization propagator is constructed using the UHF propagators which do not contain the low energy scale, and hence are flat for $\tilde{\omega}_{h\sigma} \sim \mathcal{O}(1)$, the strong coupling (SC) asymptotics derived for the SIAM would be similar to that for the PAM. The only difference would be in the value of $\Delta_0 \sim \mathcal{O}(V^2/t_*)$ since the UHF propagators for the PAM have a different structure than that of the SIAM. Using equations (3.7) and (3.8) in (3.6), and expanding the logarithm appearing in equation (3.8) to linear order in h , we get

$$S_{KR} \xrightarrow{SC} 4h. \quad (3.9)$$

As argued in [17], the above result is synonymous to the Wilson’s ratio being equal to 2 in SC. The inset of figure 6 shows the ratio S_{KR}/h as a function of interaction strength. It is seen that even for $U \sim 2$, the ratio is ~ 3 , which implies a non-rigid shift of the spin bands. Further, with increasing interaction strength, the ratio increases monotonically. Although it must asymptotically approach 4, to be consistent with the result (equation (3.9)) obtained above, we are unable to access the large U region (for $\epsilon_c = 0.5$) due to the prohibitive computational expense in handling exponentially small low energy scales.

In a recent DMFT study using QMC as the impurity solver, the Kondo lattice model was studied [27]. Real frequency spectra were obtained with a stochastic analytic continuation method. The parameters chosen were $J = 1.6t_*$ and $n_c = 0.85$. The main result was that the bands were found to shift rigidly, in contrast to what we find above. The difference with our findings could be due to various reasons, of which the most important seems to be that their low energy scale is $0.09t_*$, while our scales are $\sim 10^{-3}t_*$ (see figure 3). This is significant because only when the Kondo scale is exponentially small is the coupling between the impurity and the conduction spin renormalized strongly, and thus the Kondo screening would be strong. If this Kondo screening is weak, as it could probably be in the study mentioned above, then the Zeeman effect would win easily, and the bands would shift rigidly.

Now, we turn our attention to field dependent transport properties. At finite temperature, as the spin summed conduction electron spectra exhibits universal scaling in terms of $T/\omega_{L\sigma}$ ($\omega_{L\sigma} = Z_{\sigma}(h)V^2/t_*$) in the strong coupling regime for low fields, we expect that the resistivity will also exhibit scaling in terms of $T/\omega_{L\sigma}$. The classic HF metallic resistivity increases with temperature (initially as T^2), goes through a maximum $T_{\max} \simeq \omega_L$ (the peak position of $\rho(T)$) and then decreases with temperature characteristic of single-impurity behaviour. We observe the same form for the resistivity in our calculations. In figure 7 (top), the resistivity versus scaled temperature $T/\omega_{L\sigma}$ is shown for both $\sigma = \uparrow, \downarrow$ and for a range of fields: $\tilde{h} = 0.0$ (solid), 0.06 (dotted), 0.5 (dashed), 0.5 (long dashed) and 2.0 (dot-dashed) with U/t_* equal to 6.6. The two most significant features of the above result are—(i) negative magnetoresistance is observed over the entire range of temperatures as shown in figure 7 (bottom). (ii) The maximum in resistivity at the coherence peak reduces in magnitude and moves to higher temperatures with increasing field. In previous work, magnetoresistance was found to be positive for the SIAM [31] through Fermi liquid theory arguments and for the Anderson lattice [13] through the average T -matrix approximation (ATA). The fundamental difference between the SIAM and the PAM is the presence of lattice coherence in the latter which manifests itself at low temperatures. At $T \gtrsim \omega_L$, it is clear that magnetic field suppresses spin-flip scattering (SFS) since the main effect of a field would be to polarize the system. However, at low temperatures, the physics is different. Kondo singlet formation in the SIAM, which at zero field, quenches the SFS and hence leads to saturation of resistivity, is inhibited at finite

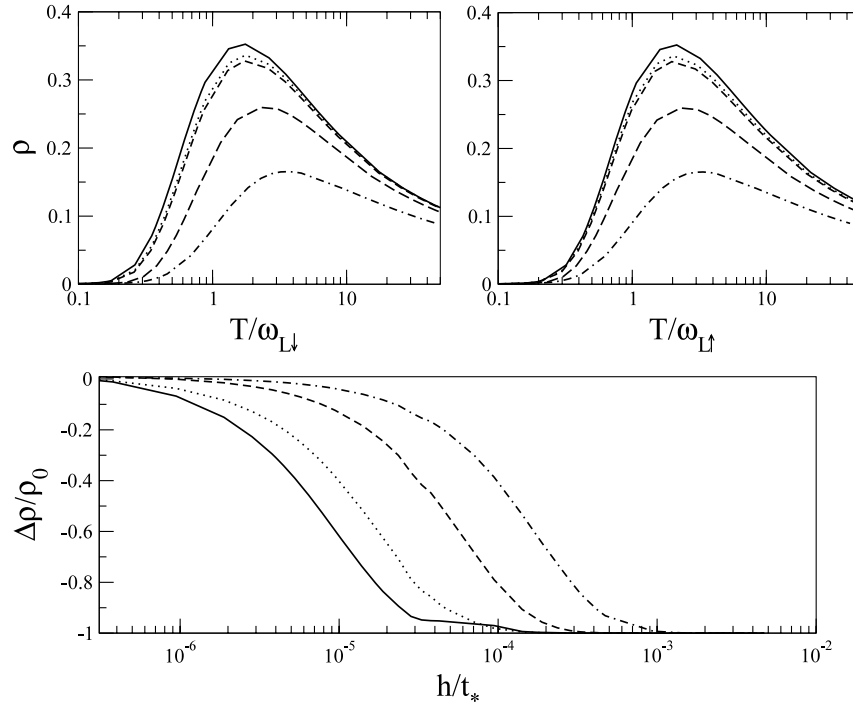


Figure 7. Top: left panel: resistivity versus $\tilde{\omega}_{h\downarrow}$ for the same parameters, but for the various fields ($\tilde{h} = 0.0$ (solid), 0.06 (dotted), 0.1 (dashed), 0.5 (long dashed) and 2.0 (dot-dashed)). Right panel: resistivity versus $\tilde{\omega}_{h\uparrow}$ for the same sets of parameters. Bottom: magnetoresistivity versus bare fields h/t_* for $U = 6.6t_*$, $\epsilon_c = 0.3t_*$ and $\eta \rightarrow 0$ for $\tilde{T} = 0.3$ (solid), 0.6 (dotted), 2.0 (dashed), 6.0 (dot-dashed).

fields, implying an increase in incoherent scattering and thus a positive magnetoresistance. In the lattice case, however, although a magnetic field does inhibit the singlet-forming screening process of local moments, the periodicity of the local moments (even though not fully screened), introduces lattice coherence which strongly suppresses incoherent scattering at low temperatures, and hence again leads to negative magnetoresistance. In other words, the incoherent scattering introduced by a magnetic field in the SIAM through the inhibition of the screening process, is countered in the PAM because of the presence of lattice/Bloch coherence. It is possible that such an effect is enhanced in the present calculation due to the use of the DMFT framework, since non-local dynamical fluctuations are completely neglected in this framework. The ATA for the Anderson lattice is in a subtle way somewhat similar to the single-site DMFT *without the self-consistency*. Which would imply that the effects of lattice coherence are probably suppressed in the ATA, and hence positive magnetoresistance is observed. Thus, we conclude that, at higher temperatures ($T \gtrsim \omega_L$), suppression of the spin-flip scattering, and at lower temperatures, the presence of lattice coherence in the PAM lead to negative magnetoresistance in the presence of a field for all T .

The shift of coherence peak to higher T with increasing field is a reflection of the increase in the low energy scale with field (see figure 3). The latter result has been obtained for the SIAM as well [17]. Since increasing interactions lead to an exponential decrease in ω_L , it appears that the polarizing effect of a magnetic field is to counter the effect of interactions, and eventually at very large fields, wipe out local moment physics (scattering/screening) completely. At temperatures

much higher than the field ($T \gg h$), the effect of a magnetic field is negligible implying that the magnetoresistance is almost zero. Next, we compare our theoretical results with experiment.

4. Comparison to CeB₆

In this section we want to compare our theoretical results with experiments on CeB₆. The rare-earth hexaboride CeB₆ has been investigated for many years [32–37]. The cubic lattice system, at low temperatures, exhibits various magnetic phase transitions between 1.6 and 3.3 K, which manifest clearly as kinks in the resistivity, above which the system is in a paramagnetic phase. It is the $T > 3.3$ K phase that we concentrate on, since our approach does not describe the symmetry broken states. Although there have been extensive studies of this material, the most detailed magnetoresistance study was carried out by Takase *et al* [32], who measured the resistivity of a CeB₆ single crystal in the temperature range from 3 to 300 K and up to magnetic field 85 kOe. We use their data for comparison to our theory.

From an earlier study [21], it is known that the HF system CeB₆ belongs to the moderately strong coupling regime. Hence we have taken the theoretical results to compare with experiments on CeB₆ for the following parameters: $U = 2.4t_*$, $\epsilon_c = 0.5t_*$, $\eta \rightarrow 0$ and $V^2 = 0.2t_*^2$. The experimental resistivity for zero field shown in the left panel of figure 8 (data from [32]) is characteristic of classic HF metals. The resistivity rises sharply from a low value, going through a coherence peak at $T \sim 4$ K, and subsequently decreasing through a small log-linear regime. At higher temperatures [21, 33] (not shown), resistivity exhibits single-impurity incoherent behaviour ($T \sim$

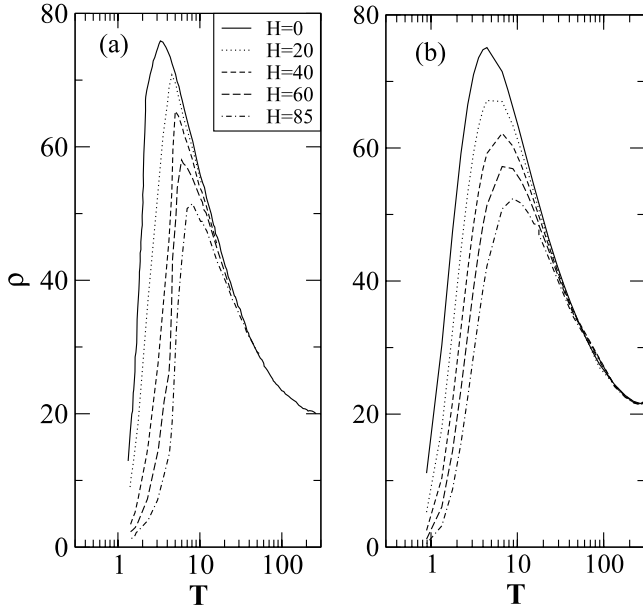


Figure 8. Resistivity versus temperature of CeB₆ (a) experiment (b) theory for the various fields: $H = 0$ kOe (solid), 20 kOe (dotted), 40 kOe (dashed), 60 kOe (long dashed) and 85 kOe (dot dashed).

100–300 K), goes through a weak minimum ($T \sim 375$ K) and finally starts increasing again like a normal metal. With increasing magnetic field, negative magnetoresistance is seen at low temperatures ($T \lesssim 50$ K) for all fields. At higher temperatures, the resistivity remains unaffected by magnetic field. This behaviour is natural and expected as discussed in section 3. The application of magnetic field results in suppression of spin–spin scattering at $T \gtrsim \omega_L$, thus causing a reduction in resistivity. At low temperatures lattice coherence takes over and the magnetoresistance stays negative. In the strong coupling regime, the effect of a magnetic field (H) should be expected to extend to temperatures, which are of a similar magnitude i.e. $T \sim g\mu_B H/k_B$, which in the experiment corresponds to ~ 5.6 K for $H = 85$ kOe (see next paragraph). However, the highest field affects the resistivity up to a temperature of ~ 50 K. Such behaviour is characteristic of the intermediate coupling regime [20], which is consistent with the model parameters for CeB₆.

To compare the experimental results with our theory, two fundamental requirements need to be met. The first requirement is that we should extract the contribution to the measured resistivity from phonons ($\rho_{\text{ph}}(T)$) and the residual resistivity ($\rho(0)$). This is given by $\rho_{\text{mag}}^{\text{exp}}(T) = a(\rho(T) - \rho(0)) - \rho_{\text{ph}}(T)$, where a is a constant which comes from the error of the sample geometry to the measured resistivity. A detailed discussion of this point is given in [21]. In this work, we simply assume $a = 1$. The second requirement is that the value of the low energy scale is needed for comparing our theoretical results with experiment. For this, we superposed the theoretical resistivity $\rho_{\text{mag}}(T)$ onto $\rho_{\text{mag}}^{\text{exp}}(T)$ for $h = 0$ to calculate the value of the low energy scale. The value of the low energy scale turns out to be $\omega_L = 2.2$ K. Assuming the g -factor to be roughly unity, the magnetic field of 1 kOe can be translated into multiples of the low energy scale. For

$H = 1$ kOe, $\frac{1}{2}g\mu_B H \simeq 0.033$ K $\simeq 0.015\omega_L$. Thus the magnetic fields employed in the experiments [32] turn out to be (in multiples of ω_L), $\tilde{h} = 0, 0.3, 0.6, 0.9$ and 1.25 , corresponding to fields of $H = 0, 20$ kOe, 40 kOe, 60 kOe and 85 kOe respectively. So, given the model parameters and the low energy scale, along with the temperature range and the field range, we can compute the resistivity as a function of temperature at the same fields as in the experiment.

With a simple multiplicative scaling of the theoretical resistivities on the x -axis by the low energy scale and the y -axis by a single multiplicative factor (the same for all fields), we show the theoretical computed dc resistivities for the same magnetic fields as the experiment in the right panel of figure 8. The experimental resistivity is found to rise more steeply than the theoretical one. The magnitude of magnetoresistivity is found to be higher in theory than the experiment. Nevertheless the functional form agrees quite well. At $T \gtrsim 50$ K, the magnetic field is seen to have very little effect on the resistivity, both in theory and experiment. Below 50 K, the magnetoresistance in the theory is negative, which is also in agreement with experiment. The coherence peak is seen to move to higher T with an increase in field; a behaviour seen in the experiment as well. The small log–linear regime that appears at temperatures higher than the coherence peak temperature is also reproduced in the theory. Thus, when compared with the experimental results in figure 8, good qualitative agreement is found between theory and experiment.

5. Conclusions

In summary, we have employed a non-perturbative local moment approach to the asymmetric periodic Anderson model within DMFT in the presence of a magnetic field. The field dependent dynamics and transport properties of the model have been computed. In the strong coupling Kondo lattice regime of the model, the local c - and f -electron spectral functions are found to exhibit universal scaling, being functions solely of $\omega/\omega_{L\sigma}$, $T/\omega_{L\sigma}$ ($\omega_{L\sigma}$ being the low energy scale) for a given effective field h_{σ}^{eff} . Although the externally applied field is globally uniform, the effective local field experienced by the c - and f -electrons differs because of correlation effects. Fermi liquid behaviour has been established even in the presence of magnetic fields through adiabatic continuity to the non-interacting limit. In the presence of a magnetic field, the quasiparticle peak at $h = 0$ and $T = 0$ splits into two. The shift of these peaks away from the Fermi level is not rigid due to the competition between local moment screening and Zeeman spin polarization. Although these shifts vary linearly with the field in strong coupling, the slope is enhanced as compared to the non-interacting limit. Finally, a comparison of theoretical magnetoresistance results with those of CeB₆, measured experimentally, yields good agreement.

Acknowledgments

We would like to thank Professor David E Logan for extremely fruitful discussions, and the Department of Science and Technology, India for funding.

References

- [1] Grewe N and Steglich F 1991 *Handbook on the Physics and Chemistry of Rare Earths* vol 14, ed K A Gschneider Jr and L Eyring (Amsterdam: Elsevier)
- Hewson A C 1993 *The Kondo Problem to Heavy Fermions* (Cambridge: Cambridge University Press)
- Stewart G R 2001 *Rev. Mod. Phys.* **73** 797
- [2] Vollhardt D 1993 *Correlated Electron Systems* vol 9, ed V J Emery (Singapore: World Scientific)
- Pruschke T, Jarrell M and Freericks J K 1995 *Adv. Phys.* **44** 187
- Georges A, Kotliar G, Krauth W and Rozenberg M J 1996 *Rev. Mod. Phys.* **68** 13
- Gebhard F 1997 *The Mott Metal–Insulator Transition (Springer Tracts in Modern Physics vol 137)* (Berlin: Springer)
- [3] Jarrell M 1995 *Phys. Rev. B* **51** 7429
- Tahvildar-Zadeh A N, Jarrell M and Freericks J K 1998 *Phys. Rev. Lett.* **80** 5168
- Tahvildar-Zadeh A N, Jarrell M, Pruschke T and Freericks J K 1999 *Phys. Rev. B* **60** 10782
- [4] Pruschke T, Bulla R and Jarrell M 2000 *Phys. Rev. B* **61** 12799
- [5] Rozenberg M J, Kotliar G and Kajueter H 1996 *Phys. Rev. B* **54** 8452
- Vidhyadhiraja N S, Tahvildar-Zadeh A N, Jarrell M and Krishnamurthy H R 2000 *Europhys. Lett.* **49** 459
- [6] Grewe N, Pruschke T and Keiter H 1998 *Z. Phys. B* **71** 75
- Pruschke T and Grewe N 1989 *Z. Phys. B* **74** 439
- [7] Logan D E, Eastwood M P and Tusch M A 1997 *J. Phys.: Condens. Matter* **9** 4211
- [8] Vidhyadhiraja N S and Logan D E 2004 *Eur. Phys. J. B* **39** 313–34
- [9] News D M and Read N 1987 *Adv. Phys.* **36** 799
- Sun S J, Yang M F and Hong T M 1993 *Phys. Rev. B* **48** 16123
- Burdin S, Georges A and Grepel D R 2000 *Phys. Rev. Lett.* **85** 1048
- [10] Rozenberg M J 1995 *Phys. Rev. B* **52** 7369
- [11] Schweitzer H and Czycholl G 1989 *Solid State Commun.* **69** 179
- Schweitzer H and Czycholl G 1991 *Phys. Rev. Lett.* **67** 3724
- [12] Rice T M and Ueda K 1986 *Phys. Rev. B* **34** 6420
- Fazekas P and Brandow B H 1987 *Phys. Scr.* **36** 809
- Fazekas P 1987 *J. Magn. Magn. Mater.* **63/64** 545
- [13] Cox D L and Grewe N 1988 *Z. Phys. B* **71** 321
- [14] Logan D E, Eastwood M P and Tusch M A 1988 *J. Phys.: Condens. Matter* **10** 2673
- [15] Glossop M T and Logan D E 2002 *J. Phys.: Condens. Matter* **14** 673
- Dickens N L and Logan D E 2001 *J. Phys.: Condens. Matter* **13** 4505
- [16] Logan D E and Dickens N L 2002 *J. Phys.: Condens. Matter* **14** 3605
- [17] Logan D E and Dickens N L 2001 *Europhys. Lett.* **54** 227
- [18] Logan D E and Dickens N L 2001 *J. Phys.: Condens. Matter* **13** 9713
- Logan D E and Glossop M T 2002 *J. Phys.: Condens. Matter* **12** 985
- Glossop M T and Logan D E 2003 *J. Phys.: Condens. Matter* **15** 7519
- Glossop M T and Logan D E 2003 *Europhys. Lett.* **61** 810
- Bulla R, Glossop M T, Logan D E and Pruschke T 2000 *J. Phys.: Condens. Matter* **12** 4899
- Smith V E, Logan D E and Krishnamurthy H R 2003 *Eur. Phys. J. B* **32** 49
- [19] Vidhyadhiraja N S, Smith V E, Logan D E and Krishnamurthy H R 2003 *J. Phys.: Condens. Matter* **15** 4045
- [20] Logan D E and Vidhyadhiraja N S 2005 *J. Phys.: Condens. Matter* **17** 2935
- [21] Vidhyadhiraja N S and Logan D E 2005 *J. Phys.: Condens. Matter* **17** 2959
- [22] Kauch A and Byczuk K 2006 *Physica B* **378–380** 297
- [23] Saso T 1997 *J. Phys. Soc. Japan* **66** 1175
- [24] Beach K S D, Lee P A and Monthoux P 2004 *Phys. Rev. Lett.* **92** 026401
- [25] Parihari D, Vidhyadhiraja N S and Logan D E 2008 *Phys. Rev. B* **78** 035128
- [26] Viola S K, Beach K S D, Castro Neto A H and Campbell D K 2008 *Phys. Rev. B* **77** 094419
- [27] Beach K S D and Assaad F F 2008 *Phys. Rev. B* **77** 205123
- [28] Graf T, Movshovich R, Thompson J D, Fisk Z and Canfield P C 1995 *Phys. Rev. B* **52** 3099
- [29] Chen C, Li Z-Z and Xu W 1993 *J. Phys.: Condens. Matter* **5** 95
- Chen C and Li Z-Z 1994 *J. Phys.: Condens. Matter* **6** 2957
- [30] Luttinger J M and Ward J C 1960 *Phys. Rev.* **118** 1417
- [31] Hewson A C, Bauer J and Koller W 2006 *Phys. Rev. B* **73** 045117
- [32] Takase A, Kojima K, Komatsubara T and Kasuya T 1980 *Solid State Commun.* **36** 461
- [33] Sato N, Sumiyama A, Kunii S, Nagano H and Kasuya T 1985 *J. Phys. Soc. Japan* **54** 1923
- [34] Marcenat C, Jaccard D, Sierro J, Floquet J, Onuki Y and Komatsubara T 1990 *J. Low Temp. Phys.* **78** 261
- [35] Kimura S I, Nanba T, Kunii S and Kasuya T 1994 *Phys. Rev. B* **50** 1406
- [36] Nakamura S, Goto T and Kunii S 1995 *J. Phys. Soc. Japan* **64** 3491
- [37] Goodrich R G *et al* 2004 *Phys. Rev. B* **69** 054415